Mon. Not. R. Astron. Soc. **269**, 462–474 (1994)

On the possible stellar origin of the optical variability of NGC 4151

Itziar Aretxaga[1]★ and Roberto Terlevich[2]

[1] *Dpto Física Teórica, C-XI, Universidad Autónoma de Madrid, E-28049 Cantoblanco, Madrid, Spain*
[2] *Royal Greenwich Observatory, Madingley Road, Cambridge CB3 0EZ*

Accepted 1994 March 4. Received 1994 February 23; in original form 1992 November 4

ABSTRACT

It has been suggested that the activity seen in many active galactic nuclei (AGN) may be powered solely by young stars and compact supernova remnants in a nuclear burst of star formation. Owing to its proximity and historically well-sampled light curve, the type 1 Seyfert NGC 4151 is, among galaxies with AGN, the best candidate to test the origin of the observed long-term nuclear variability in low-luminosity AGN.

We find that the energies and light curves of observed supernovae (SNe) and compact supernova remnants (cSNRs) are similar to those of the isolated variations of the nucleus of NGC 4151.

Two strong predictions, valid for 10- to 60-Myr-old high-metallicity starbursts, are discussed. (i) The number of peaks of the light curve, or supernova rate, is uniquely related to the nuclear luminosity during the minimum of the light curve. This result is almost independent of the initial mass function, age and/or total mass of the cluster. For NGC 4151, the minimum luminosity $M_B = -19.5$ mag indicates an SN rate $\nu_{SN} = 0.2$–$0.3\ \mathrm{yr}^{-1}$. (ii) The time-averaged equivalent width of Hβ ($\overline{W_{H\beta}}$) is related to the total energy of the SN, almost independently of the initial mass function, age and/or total mass of the cluster and, furthermore, independently of the assumed cosmology. As a corollary, we conclude that the narrow range of observed values of $\overline{W_{H\beta}}$ in AGN that show broad emission lines is a direct consequence of the universal value of the energy released in an SN explosion. For NGC 4151, $\overline{W_{H\beta}} = 78$ Å gives an energy per SN of 3×10^{51} erg.

Monte Carlo simulations of the light curve are presented. Each of the three input parameters of the models, the SN rate, the total energy per SN and the density of the circumstellar medium, is well constrained by two independent sets of observations. The variability of the object fulfils the predictions of the model. The simulated light curves are remarkably similar to the observed one. The best fit of the simulated light curves to that of NGC 4151 is also produced for a supernova rate $\nu_{SN} \approx 0.2$–$0.3\ \mathrm{yr}^{-1}$, an energy per SN of about 3×10^{51} erg, and a cSNR circumstellar density of about $10^7\ \mathrm{cm}^{-3}$.

Key words: supernovae: general – galaxies: active – galaxies: individual: NGC 4151 – galaxies: nuclei – galaxies: Seyfert – galaxies: starburst.

1 INTRODUCTION

In the starburst model, the variability observed in radio-quiet active galactic nuclei (AGN), i.e. Seyfert galaxies and most optically selected quasars, is thought to be produced by the supernova (SN) and compact supernova remnant (cSNR) activity resulting from the evolution of a metal-rich massive stellar cluster, the product of a starburst in the nucleus of an early-type galaxy (Terlevich, Melnick & Moles 1987; Terlevich et al. 1992). The observed multifrequency spectrum of such a radio-quiet AGN is reproduced by the combined contribution of stars, SNe, cSNRs and dust which are present in a stellar cluster 10 to 60 Myr old (Terlevich 1990). Most of the optical/UV and bolometric nuclear luminosity is provided by the young stars, while the cSNRs are responsible for the observed nuclear variability and characteristic broad-line spectrum. Young stellar clusters, with ages less than 10 Myr, can account for the emission-line spectra (Terlevich & Melnick 1985; Cid Fernandes et al.

★ Present address: Royal Greenwich Observatory, Madingley Road, Cambridge CB3 0EZ.

1992; Filippenko & Terlevich 1992; Shields 1992) and for the overall UV/optical/IR spectral energy distribution (García-Vargas et al. 1993) of LINER and type 2 Seyfert nuclei. The broad lines observed in some LINERs, type 1 Seyferts and QSOs are produced in cSNRs, due to the interaction of the ejecta of SNe with a high-density circumstellar medium. The intrinsic parameters of the broad-line region (BLR) can be obtained from theoretical models of cSNRs (Terlevich et al. 1992), while the observed delays of the response of the broad emission lines to the variations of the continuum have proven to be well explained by thermal instabilities during shell formation in cSNRs (Terlevich et al. 1993). The observational data that more strongly support the cSNR origin of the BLR and its variability are the properties of the 'Seyfert 1-like' supernovae SN 1987F and SN 1988I (Filippenko 1989), SN 1983K (Terlevich & Melnick 1988) and SN 1988Z (Stathakis & Sadler 1991; Turatto et al. 1993).

The observed variability of AGN is a key aspect, directly related to the source of energy, and must be explained by any model of AGN. The best information regarding variability in AGN is provided by a small group of nearby low-luminosity type 1 Seyferts. The light curves of many type 1 Seyferts show two distinct components: an occasional sharp peak variation superimposed on to a long-term recurrent modulation (Lyutyi 1977, 1979; Penston et al. 1981; Gill et al. 1984; Dibaĭ & Lyutyi 1984; Alloin et al. 1986; Lyutyi & Oknyanskii 1987; Pica et al. 1988; Snijders 1991; Ulrich et al. 1991; Smith, Nair & Clemens 1991; Smith et al. 1993), hereinafter called rapid and slow components, respectively (see Smith et al. 1991 for a schematic picture). The peaks of the rapid component last some weeks, while the cycles of the slow one are a few years long. Alloin et al. (1986) found that the total energy radiated by a complete slow-component variation is about 10^{51} erg, while individual flares emit energies of about 10^{49}–10^{50} erg. In the starburst model, the slow component is related to the long-term behaviour of cSNRs, while the rapid component is mostly due to cool instabilities in the shells of cSNRs and to SN flashes. The processes that occur prior to thin shell formation in a rapidly radiating supernova remnant, i.e. as it achieves maximum luminosity, produce time delays between the continuum and line emissions, line and continuum luminosities, and emission-line ratios with values similar to those observed in low-luminosity AGN (Franco et al. 1993; Tenorio-Tagle et al. 1993). After shell formation, the remnant produces, through cooling instabilities, secondary fainter flares with little or no lag between the continuum and the lines. These results have been compared, in a separate paper (Terlevich et al. 1994), with the 'AGN Watch' extensive monitoring campaign on NGC 5548 (Clavel et al. 1991; Peterson et al. 1991), to show that the compact supernova remnant model is able to give an accurate and detailed description of the temporal behaviour of the BLR, as well as to account for all of its intrinsic parameters with essentially just one free parameter: the density of the ambient medium ($\approx 10^7$ cm^{-3}). The long-term variability of NGC 5548 can be described by similar models to those presented here (Aretxaga & Terlevich 1993), but the test of the starburst model given by this object is not as critical as that given by NGC 4151, since the light curve of NGC 5548 is not so well sampled for time-scales $\gtrsim 10$ yr. Only since the beginning of the 'AGN Watch' campaign has good sampling been available for NGC 5548, but this, so far, only covers one complete long-term event.

In the present paper, we concentrate on the slow-component variations: the number and amplitude of the peaks, and their relationship with the minimum luminosity. We show that a starburst 10–60 Myr old can reproduce the overall pattern of the optical light curve of the extensively monitored type 1 Seyfert NGC 4151, and explain its nuclear luminosity in a self-consistent way. In Section 2, the shape of the best-sampled peak in the light curve of NGC 4151 is compared with some light curves of SNe. In Section 3, we estimate the rate of SN explosions that should be observed in the nucleus of NGC 4151, if the light detected in the less active stages, corresponding to the minima of the light curve, arises from a young stellar cluster. In Section 4, we simulate a light curve with the previously deduced SN rate and compare it with the observed light curve of NGC 4151. In Section 5, the self-consistency of the model is discussed. Section 6 summarizes the main conclusions of this work.

2 COMPARING THE LIGHT CURVE OF NGC 4151 WITH THOSE OF TYPE II SUPERNOVAE

2.1 NGC 4151: parameters

NGC 4151 [$\alpha(1950.0) = 12^h\ 8^m\ 1^s$, $\delta(1950.0) = +39°\ 41'\ 2''$, $v_r = 978$ km s^{-1} (Sandage & Tammann 1981)] has been considered to be the prototype Seyfert 1, although the lack of broad lines in some epochs shows that this galaxy can transit between Seyfert types 1 and 2 in a relatively short time of about one month to one year (Penston & Pérez 1984; Lyutyi, Oknyanskii & Chuvaev 1984). NGC 4151 is about 28° away from the centre of the Virgo cluster, $\alpha(1950.0) \approx 12^h\ 30^m$, $\delta(1950.0) \approx 12°\ 40'$. This proximity to the Virgo cluster implies that a fraction of the observed redshift of NGC 4151 is due to the radial component of its infall velocity towards the cluster. Owing to this effect, galaxies in front of Virgo have, on average, recession velocities higher than those corresponding to the isotropic Hubble flow and, conversely, galaxies behind Virgo have recession velocities lower than those of the Hubble flow. NGC 4151 is in this second group and, as a result, the galaxy is further away than inferred from the Hubble relation. To improve the estimation of the distance to NGC 4151, we modelled the Virgo infall velocity field. For a median redshift of Virgo of 950–1120 km s^{-1} and a Local Group infall into the Virgo cluster of 200–300 km s^{-1} (Dressler et al. 1987), the corrected recession velocity of NGC 4151 is $v_c \approx 1330 \pm 200$ km s^{-1} (27 ± 4 Mpc for $H_0 = 50$ km s^{-1} Mpc^{-1}), where the uncertainty indicates the range of adopted parameters in the model. This corrected distance implies an increase in the absolute magnitude of NGC 4151 of 0.67 mag, with respect to the uniform Hubble expansion case.

2.2 NGC 4151: light curve

The observed blue light curve of the nucleus of NGC 4151 is presented in Fig. 1. The data were collected by M. V. Penston & M. A. J. Snijders (private communication; see also Snijders 1991) from different sources. The light curve shows occasional sharp variations that last some weeks, which constitute the rapid component of variation, and bumps 2–5 yr long, which constitute the slow component of variation.

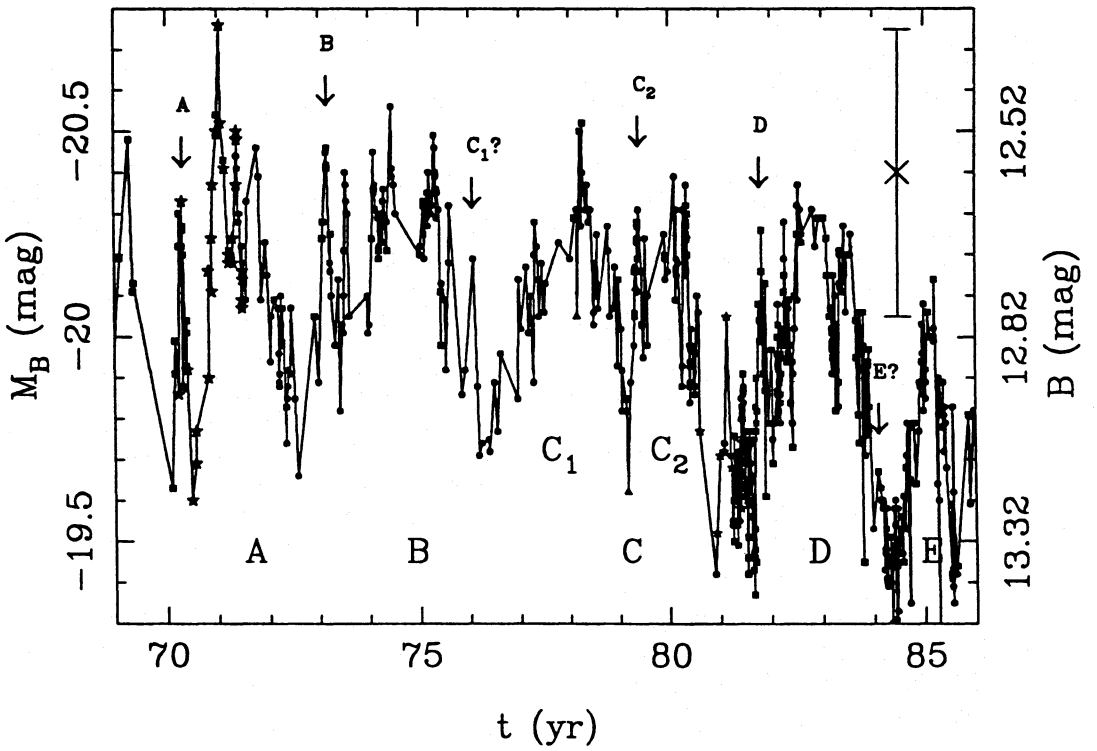

Figure 1. Light curve of NGC 4151 in absolute *B* magnitudes. Data collected by M. V. Penston & M. A. J. Snijders (private communication). Different symbols correspond to different optical photometries. The uncertainties in the derivation of the radial velocity of the galaxy are shown by the point with an error bar at the upper right corner of the panel.

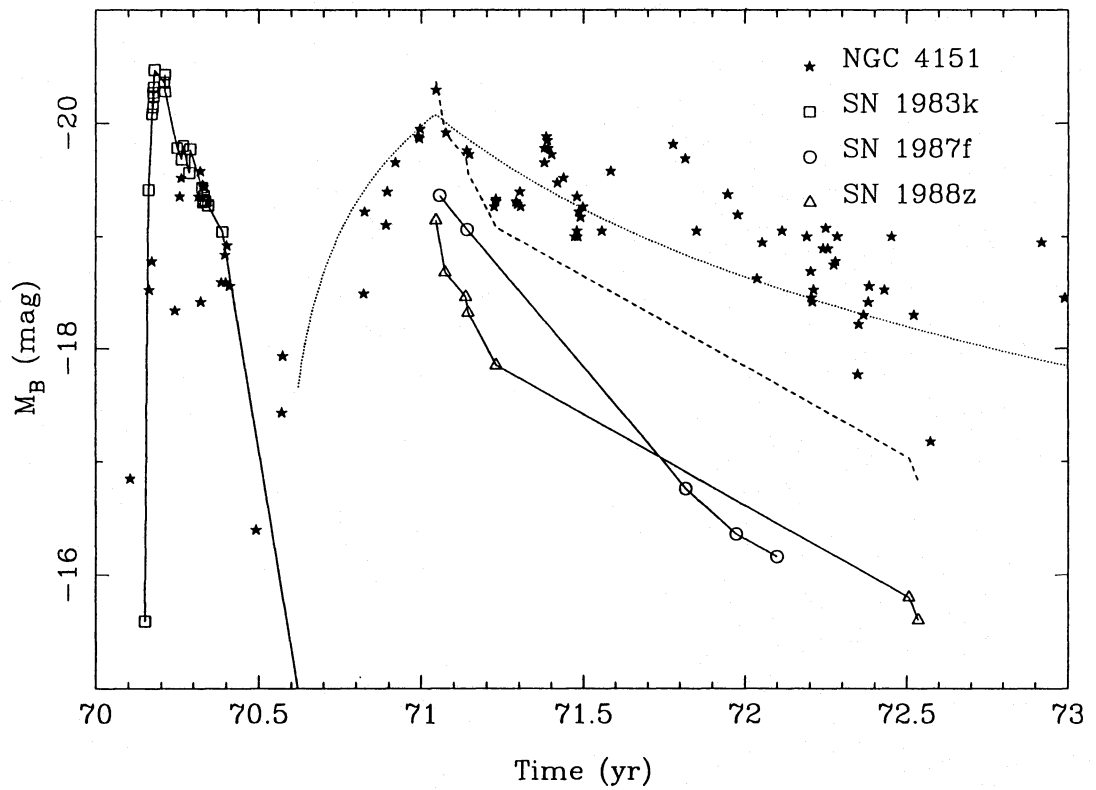

Figure 2. Comparison of the net variation of the light curve of NGC 4151, in absolute *B* magnitudes, to the light curves of supernovae SN 1983K, 1987F and 1988Z. The dotted line reproduces the theoretical *B*-band light curve for a cSNR ($\varepsilon_{51} = 3$, $n_7 = 1$) used in the simulations of Section 4. The dashed line represents the light curve of SN 1988Z, scaled to match the second maximum of the figure.

The first well-sampled rapid- and slow-component variations occurred between 1970 and 1973. The maximum in 1971 corresponds to the brightest well-sampled slow-component variation of the whole light curve. Although that of 1974/75 is, perhaps, almost as bright, its sampling is not as good. In the last few years, there have been several spectroscopic monitoring campaigns on NGC 4151 (Clavel et al. 1990; Maoz et al. 1991), and although they have been very useful in determining certain aspects of the rapid variability, such as the lag of the lines, they have failed to trace a single and complete slow-component cycle.

The 1970–73 light curve is shown expanded in Fig. 2. The filled stars show the absolute blue magnitude of the variable component of the nucleus, computed assuming that the minimum of the light curve, $m_B \approx 13.5$ mag or $M_B \approx -19.5$ mag in 1984, corresponds to an underlying non-variable nuclear component. The extinction in NGC 4151 was taken to be $A_B = 0.66$ mag, as derived from emission-line ratios and from the nuclear infrared luminosity (Rieke & Lebofsky 1981).

The complete light curve during this period has two distinct maxima, separated by a deep minimum. The first event lasts for a few weeks and shows a rapid decline, while the second lasts for more than a year and presents a slow decline with at least two secondary maxima. This latter characteristic of the long event, the decay of a few years with several secondary maxima, looks similar to the recurrent bursts observed in the light curve of NGC 1566 (Alloin et al. 1986).

2.3 cSNR variability

A double-peaked variation, similar to that in Fig. 2, is expected to occur in the light curve of an SN evolving in a high-density circumstellar medium. The first peak would correspond to the SN flash, and the second would correspond to the time when the cSNR reaches the maximum of its radiative phase (Wheeler, Mazurek & Sivaramakrishnan 1980; Shull 1980; Terlevich et al. 1992). The time between the explosion and the start of the radiative phase is

$$t_{sg} \approx 0.62 \text{ yr } \varepsilon_{51}^{1/8} n_7^{-3/4}, \quad (1)$$

where ε_{51} is the energy of the cSNR in units of 10^{51} erg, and n_7 is the circumstellar density in which this cSNR evolves, in units of 10^7 cm^{-3}. During the radiative phase, the luminosity of the remnant is

$$L_{bol}(t) \approx 2 \times 10^{43} \text{ erg s}^{-1} \varepsilon_{51}^{7/8} n_7^{3/4} \left(\frac{t}{t_{sg}}\right)^{-11/7}, \quad (2)$$

emitted mainly in the far-UV and X-rays. Several secondary maxima associated with cooling instabilities are expected during this phase (Chevalier & Imamura 1982; Terlevich et al. 1994). These events have typical energies that are about 1–5 per cent of the total energy of the cSNR.

We compare the first peak in Fig. 2 with the light curve of the Type II supernova in NGC 4699, SN 1983K. This very bright supernova was discovered two and a half weeks before reaching its maximum (Phillips et al. 1990). The presence of narrow emission lines near the maximum and the slow initial increase in luminosity pointed to the existence of an extended circumstellar shell (Niemela, Ruíz & Phillips 1985). Comparative studies with other supernova light curves show that the progenitor star of SN 1983K could have been a red supergiant (Phillips et al. 1990), although the observed pre-maximum spectra were similar to those found in Wolf–Rayet stars (Niemela et al. 1985). The light curve of SN 1983K is presented in Fig. 2, superimposed on the first peak of NGC 4151, assuming a redshift of NGC 4699 of $v = 1511$ km s^{-1} (Barbon, Capellaro & Turatto 1989), which gives a corrected recession velocity from the Virgo infall of $v_c = 2000$ km s^{-1}, and galactic extinction $A_B = 0.07$ mag (Phillips et al. 1990).

We conclude that a supernova like SN 1983K can account for the luminosity and shape of the first peak in Fig. 2. Furthermore, Terlevich & Melnick (1988) have shown that the luminosity, duration and optical spectrum near the maximum of SN 1983K are similar to those observed during the nuclear flares of the low-luminosity type 1 Seyfert NGC 5548 (Peterson & Ferland 1986). In general, we see that the energies and light curves of some Type II SNe are similar to those of the isolated peaks in the light curve of the galactic nucleus.

The second peak of NGC 4151 in Fig. 2 has a much slower decay than that of a classical SN, but it is comparable to those observed in some recently discovered peculiar Type II supernovae. SN 1987F and 1988Z are two of these peculiar SNe (Schlegel 1990). These objects show blue-dominated continua and emission lines, with a non-variable narrow component sitting on a variable broad base. Their evolution is slow, with much flatter light curves than classical Type II with plateau, which points to the existence of extended circumstellar shells of high density (Schlegel 1990; Stathakis & Sadler 1991; Turatto et al. 1993). We identify this type of SN with cSNRs, and not with SN outbursts as hitherto assumed.

SN 1987F was discovered after maximum in a spiral arm of the Sc galaxy NGC 4615, superimposed on an H II region. The lack of broad forbidden emission lines in its spectrum suggests that the electron density of the expanding gas should be at least 10^7 cm^{-3}, probably $\sim 4 \times 10^9$ cm^{-3} (Filippenko 1989). The light curve published by Filippenko is represented in Fig. 2, assuming a recession velocity of NGC 4615 of $v = 4746$ km s^{-1} (Barbon et al. 1989). The extinction produced in the parent galaxy of the cSNR is unknown, but it could be very high, as expected from the presence of the H II region, while the galactic extinction is negligible ($b \sim 88°$).

SN 1988Z was discovered on 1988 December 14, in the galaxy M+03-28-022 (Zw 095-049), close to a probable H II region. The extinction in the parent galaxy is unknown and the galactic extinction is negligible ($b \sim 60°$). In this case, a direct measurement of the circumstellar density was possible. The value of the density, determined from the [O III] λ4363 Å to [O III] λ5007 Å forbidden line ratio, is between 4×10^6 and 1.6×10^7 cm^{-3} (Stathakis & Sadler 1991). Fig. 2 shows the V-band data of the cSNR, converted to B magnitudes using the colour at maximum, $B - V = 0.3$ mag (Stathakis & Sadler 1991), for a recession velocity of $v = 6660$ km s^{-1} (Barbon et al. 1989).

The observed light curves of SN 1987F and 1988Z can qualitatively account for the decay amplitude of the second peak in the light curve of NGC 4151. The slope of SN 1987F is steeper, but this could be due to a different circumstellar density distribution, as inferred from equation (2). The luminosities of both cSNRs are lower than that of NGC

4151, but the intrinsic extinction produced in the parent galaxies could be very high, as the SNe are embedded in H II regions.

3 ESTIMATION OF THE SUPERNOVA RATE IN YOUNG CLUSTERS

We have shown that cSNRs can account for the slow-component variations in NGC 4151, while some of the rapid flares can be produced by a contribution of SN flashes and cooling instabilities in the evolution of the cSNR. It is important to estimate how many of these cSNRs are required in order to explain the luminosity of the nucleus.

In a coeval stellar cluster, the supernova rate ν_{SN} is given by

$$\nu_{SN} = -\frac{dN}{dm}\frac{dm}{dt}, \tag{3}$$

where N, m and t denote the number of stars, mass in stars and time, respectively. The first factor on the right-hand side of equation (3) is the initial mass function (IMF),

$$dN = \xi(m)\,dm, \tag{4}$$

and the second factor gives the change with time of the initial mass of a star at the pre-supernova stage. This second factor was computed from the stellar evolutionary models of Maeder & Meynet (1988) and Maeder (1990) for solar abundance.

We calculated the supernova rate per unit cluster mass for a variety of IMFs. The results of our computations are plotted in Fig. 3(a), where the open circles show the SN rates derived from equation (3) for the solar neighbourhood IMF (Miller & Scalo 1979), parametrized as

$$\xi(m) = \begin{cases} 0.35\,M_t\,m^{-1} & \text{if } 0.3 < m < 1\ M_\odot, \\ 0.35\,M_t\,m^{-2.35} & \text{if } 1 < m < 100\ M_\odot, \end{cases} \tag{5}$$

where M_t stands for the initial mass of the cluster. Other symbols in Fig. 3(a) give ν_{SN}/M_t for several power-law IMFs of slopes $\alpha = 2$, 2.35 (Salpeter) and 3, and lower mass limits $M_l = 0.3$, 0.5, 1 and 3 $M_\odot$.

The blue luminosity emitted by the stars of the stellar cluster was estimated, assuming that it is originated in main-sequence stars. The red supergiant contribution to the B luminosity is negligible (García-Vargas 1991). The luminosity per unit mass is given by

$$\frac{L_B^*}{M_t} = \frac{1}{M_t}\int_{M_l}^{M_H} L_B^*(m)\,\xi(m)\,dm, \tag{6}$$

where $L_B^*(m)$ is the mass–luminosity relation of main-sequence stars and M_H is the mass of a star at the turn-off point. The mass–luminosity relation, $L_B^*(m)$, was taken from Allen (1973) and M_H was estimated from the models of Maeder & Meynet (1988) and Maeder (1990). Fig. 3(b) shows the L_B^*/M_t ratio for different IMFs. This ratio, like ν_{SN}/M_t, decreases with time and is similarly dependent on the assumed IMF.

A very important result is that the ratio of the supernova rate per unit mass to the blue luminosity per unit mass, ν_{SN}/L_B^*, is almost independent of the assumed IMF and is basically constant over the whole SN II phase (see Fig. 3c). This is because both quantities, the SN rate and the blue luminosity, are due to stars in a narrow mass range close to the turn-off point, and do not depend on the number of low-mass stars that make up the bulk of the mass of the cluster. Fig. 3(d) shows the SN rate as a function of the absolute blue magnitude of the stars of the cluster, for an age ≈ 40 Myr. At this age, a cluster with $M_B^* \approx -21.3$ mag will produce about 1 SN per year. Table 1 gives all the relevant ratios for a wide range of ages and IMFs.

The SN rate of NGC 4151 can be estimated, assuming that the deep minimum of the nuclear light curve represents a constant component due only to the stars of a nuclear young stellar cluster. The absence of broad lines during this stage (Lyutyi et al. 1984; Penston & Pérez 1984) guarantees that the contribution of cSNRs is negligible, with respect to that of the stars. In general, at low stages the nuclear light mainly originates in the stars of the cluster, while the cSNRs dominate during the maxima of the light curve. For a 10- to 60-Myr-old cluster with a luminosity equal to that of the photometric minimum of NGC 4151, i.e. $M_B \approx -19.5$ mag, the predicted SN rate is between 0.1 and 0.3 SN yr^{-1}, as derived from Figs 3(c) and (d). One must note that, without the correction to the recession velocity of NGC 4151, due to the infall into the Virgo cluster, the luminosity at minimum is $M_B \approx -18.8$ mag, and the predicted SN rate is, consequently, almost a factor of 2 lower.

4 NUMERICAL SIMULATIONS OF THE LIGHT CURVE

Having computed the number of SNe required to explain the nuclear luminosity during the photometric minima of NGC 4151, we will attempt to reproduce in more detail the overall pattern of variability using Monte Carlo simulations of the light curve.

Our simulations have three input parameters: the rate of SN explosions (ν_{SN}), the energy per SN (ε_{51}) and the circumstellar density in which the cSNRs evolve (n_7). We assumed that SNe are random processes under a mean rate, given by the number of stars that, for a given turn-off mass, explode as SNe (equation 3).

As we saw in Section 2, SNe evolving in a high-density circumstellar medium show a double-peaked light curve: the first maximum is the SN flash itself, and the second comes from the onset of the radiative phase of the cSNR. Type II supernovae show a wide range of peak luminosities, $M_\beta \sim -16$ to -21 mag (van den Bergh 1988). We adopt a peak luminosity for the first maximum of the light curve of $M_B = -19$ mag. The B-band light evolution of a cSNR can be estimated from equation (2), assuming a bolometric correction of such a remnant, given by

$$\frac{L_{bol}}{(\nu f_\nu)_{4200\,\text{Å}}} \sim 2, \tag{7}$$

as derived from the models of Terlevich et al. (1992), and from the data of SN 1987F and 1988Z (Filippenko 1989; Stathakis & Sadler 1991). The adopted B-band light curve then results:

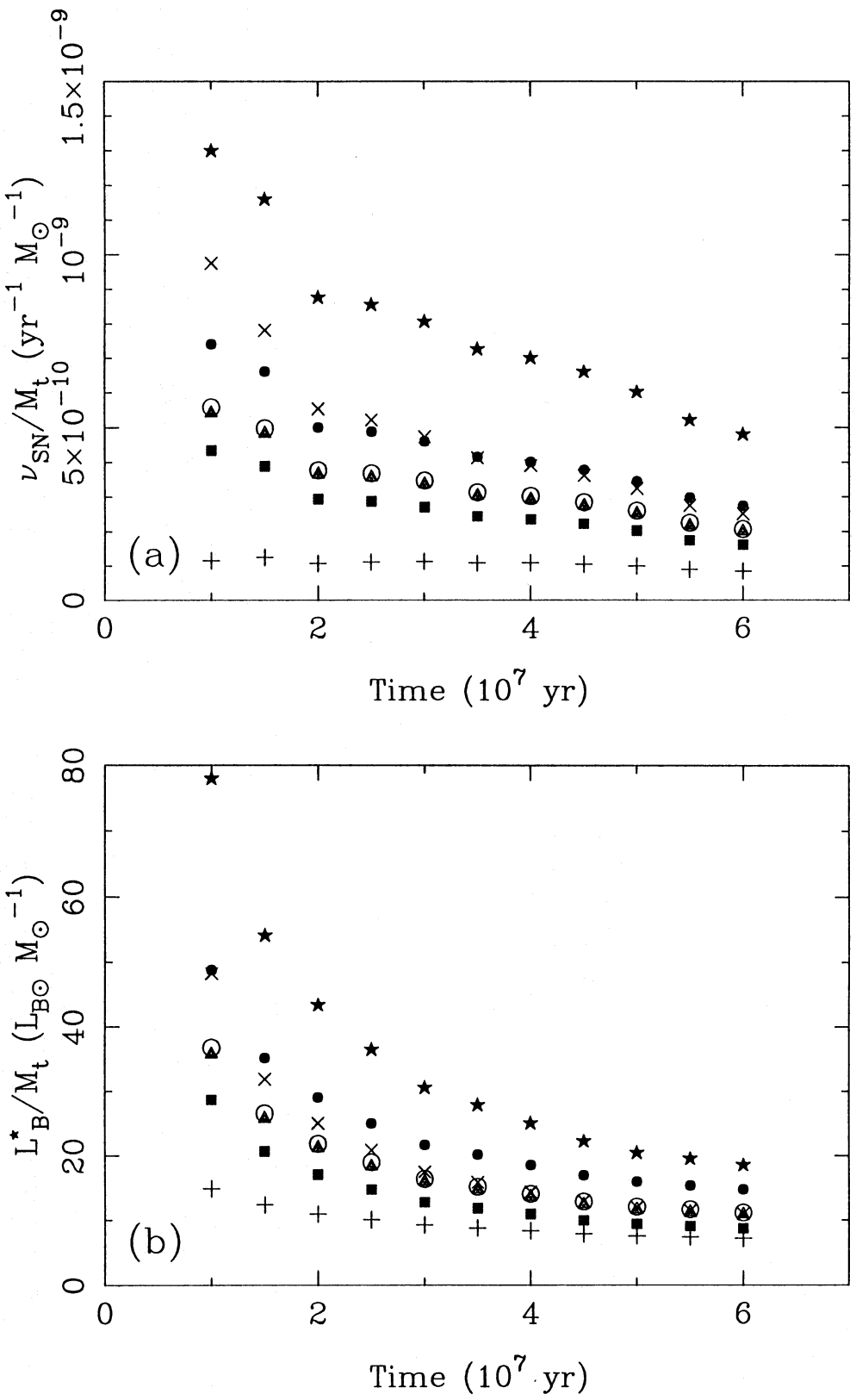

Figure 3. (a) Evolution of the ratio of the supernova rate to the total initial mass of the stellar cluster, for its SN II explosion phase. Different symbols correspond to different IMFs: open circles – Miller & Scalo's IMF with $0.3 < m < 100$ $M_\odot$; filled squares – Salpeter's IMF, with $0.3 < m < 100$ $M_\odot$; filled triangles – Salpeter's IMF, with $0.5 < m < 100$ $M_\odot$; filled circles – Salpeter's IMF, with $1 < m < 100$ $M_\odot$; filled stars – Salpeter's IMF, with $3 < m < 100$ $M_\odot$; × signs – a power-law IMF, with $\alpha = 2$, $0.3 < m < 100$ $M_\odot$; + symbols – a power-law IMF, with $\alpha = 3$, $0.3 < m < 100$ $M_\odot$. (b) Evolution of the ratio of stellar blue luminosity to total initial mass of the stellar cluster, for its SN II phase. (c) Evolution of the ratio of supernova rate to stellar blue luminosity of the cluster, for the SN II phase of the cluster. (d) Relation of supernova rate to stellar blue absolute magnitude of the cluster.

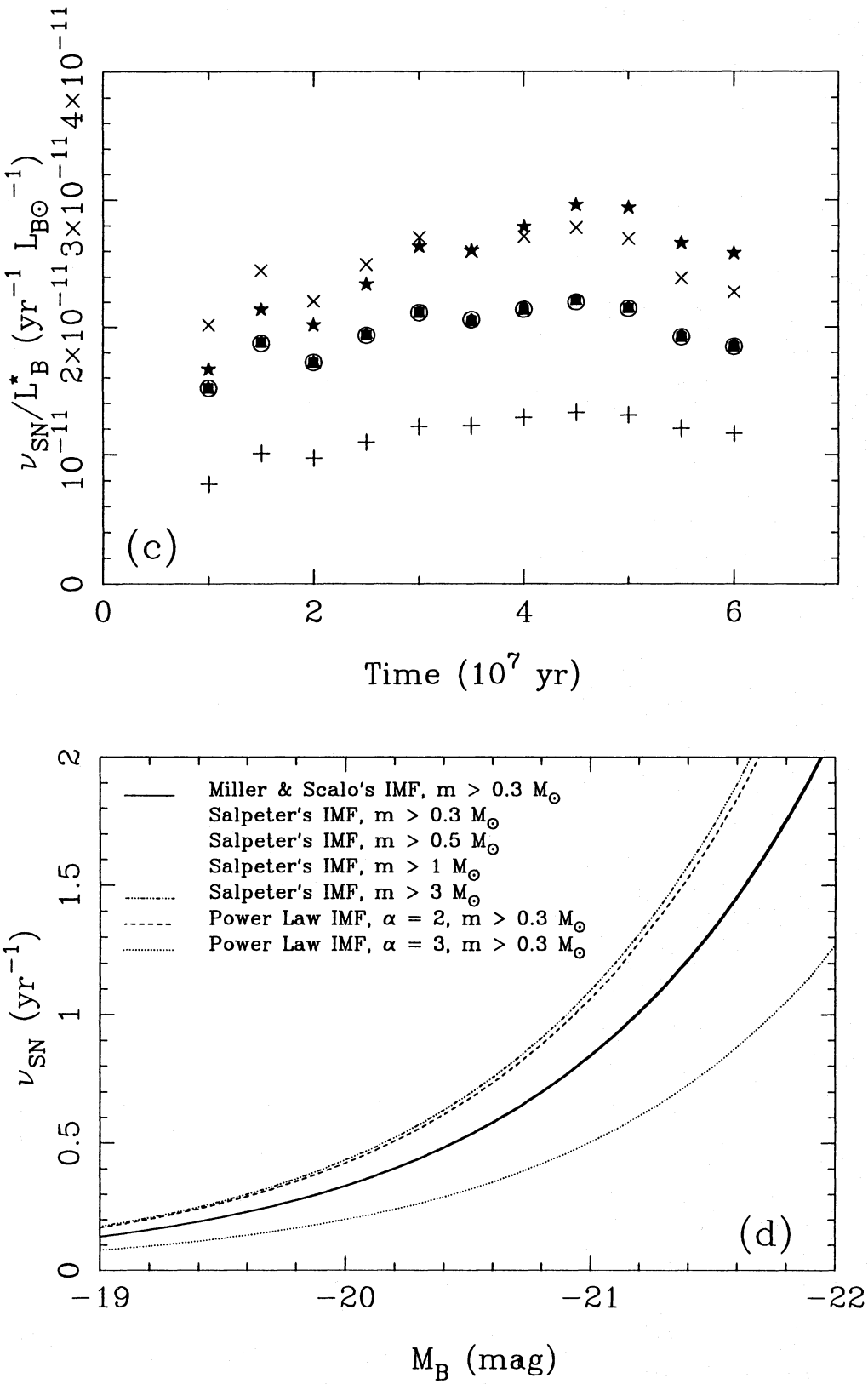

Figure 3 – *continued*

Table 1. Description of the cluster evolution. Columns: (1) time, in 10^7 yr; (2) ratio of SN rate to stellar blue luminosity, in $\mathrm{yr}^{-1}\ L_{B\odot}^{-1}$; (3) blue magnitude of the stars of a cluster with a SN rate $\nu_{SN}=1\ \mathrm{yr}^{-1}$, in mag; (4–7) ratio of stellar blue luminosity to total initial mass of the cluster, for several power-law IMFs, of slope $\alpha=2.35$ and lower mass limits M_1, in solar units; (8) initial mass of the stars undergoing SN explosions, in solar units.

t_7	ν_{SN}/L_B^*	M_B^*	L_B^*/M_t for $\alpha=2.35$				M_{SN}
			$M_1=0.3\ M_\odot$	$M_1=0.5\ M_\odot$	$M_1=1\ M_\odot$	$M_1=3\ M_\odot$	
1.0	0.15×10^{-10}	−21.7	28.70	36.80	48.80	78.00	19.8
2.0	0.17×10^{-10}	−21.5	17.10	21.90	29.10	43.40	12.1
3.0	0.21×10^{-10}	−21.3	12.80	16.40	21.70	30.60	9.8
4.0	0.21×10^{-10}	−21.3	11.00	14.10	18.60	25.10	8.4
5.0	0.21×10^{-10}	−21.3	9.44	12.10	16.00	20.50	7.6
6.0	0.18×10^{-10}	−21.4	8.78	11.20	14.80	18.60	6.9

$$L_B=\begin{cases}6\times10^9\,L_{B\odot} & \text{if } t=0,\\ 0 & \text{if } t=110\text{ d}\end{cases}\Bigg\}\ \text{first peak}$$
$$\begin{cases}0 & \text{if } t=90\text{ d},\\ 6\times10^9\,L_{B\odot}\varepsilon_{51}^{7/8}n_7^{3/4}(t/t_{sg})^{-11/7} & \text{if } t\geq t_{sg}.\end{cases}\Bigg\}\ \text{second peak} \qquad (8)$$

For simplicity, linear interpolation is used between 0 and 110 d for the first peak, and 90 d and t_{sg} for the second one. The zero-point in the time-scale corresponds to the peak of the SN outburst, and t_{sg} is defined by equation (1). The dotted line in Fig. 2 plots this theoretical B-band light curve for $\varepsilon_{51}=3$ and $n_7=1$, taking the time origin at the first maximum. It is important to note how closely the theoretical curve matches the observations. No attempt to reproduce the secondary peaks observed in this decline has been made, since we are using a simple analytical solution for the long-term behaviour of the light curve of a cSNR (see the Introduction and Section 4.1 about departures from this simplifying assumption).

To construct the model light curve of an AGN, light curves defined by equation (8) were combined using a random number generator to determine the time of explosion for a range of rates $\nu_{SN}=0.1$–1 SN yr^{-1}. The final luminosity curve includes, in a self-consistent way, the cluster luminosity, as defined by the relation shown in Fig. 3(d). To simulate the observational uncertainties of the light curve of NGC 4151, Gaussian errors were introduced with $\sigma^{obs}\sim0.1$ mag.

Three parameters were measured from the simulated light curve: the mean luminosity $\overline{M_B}$, the rms $\sigma(M_B)$, and the peak-to-peak variation ΔM_B. The parameters were estimated for five-year intervals, and for a range of cSNR parameters ($\varepsilon_{51}=1$, 3, 10; $n_7=0.5$, 1, 3, 10). The results are shown in Figs 4(a)–(c).

We can now compare the results of these simulations with the parameters of the observed light curve. The mean luminosity $\overline{M_B}$, the rms $\sigma(M_B)$ and the peak-to-peak variation ΔM_B were determined from the observed light curve of NGC 4151 for five-year intervals:

$\overline{M_B}=-20.0\pm0.22$ mag,

$\sigma(M_B)=0.24\pm0.02$ mag,

and

$\Delta M_B=1.07\pm0.07$ mag.

These values are shown in Figs 4(a)–(c) as boxes, where the box widths indicate the uncertainties in the determination. The comparison of data and models shows that the simulations that simultaneously best fit the range of observed parameters in the light curve of NGC 4151 are those for

$\nu_{SN}\approx0.2$–$0.3\ \mathrm{yr}^{-1}$,

$\varepsilon_{51}\approx3$,

and

$n_7\approx0.5$–1.

Some simulated light curves, for (a) $\nu_{SN}=0.2\ \mathrm{yr}^{-1}$, $\varepsilon_{51}=3.0\pm0.9$ and $n_7=0.5\pm0.1$, (b) $\nu_{SN}=0.3\ \mathrm{yr}^{-1}$, $\varepsilon_{51}=3.1\pm0.9$ and $n_7=1.0\pm0.3$, are shown in Figs 5(a) and (b), and should be compared with the observed light curve of Fig. 1. The parameters ε_{51} and n_7 in these simulations were allowed to vary randomly inside the limits indicated above, to take into account possible differences in the circumstellar medium, opacities and bolometric corrections of the remnants associated with different SNe.

4.1 Comparison with the observed light curve of NGC 4151

The simulations of Figs 5(a) and (b) reproduce the observed number and amplitude of the peaks of the light curve of NGC 4151, and its mean luminosity. The simulation shown in Fig. 5(b) is 0.5 mag more luminous than the general level of NGC 4151. This difference is, however, inside the uncertainties in the derivation of the absolute magnitude of the source. The error bars in Fig. 1 represent the uncertainty in the absolute magnitude scale, which can be shifted ±0.5 mag, depending on the infall model towards the Virgo cluster considered in Section 2.1. Fig. 5(b) is the simulated light curve that resembles more closely the observed one.

In Fig. 1 we have marked, with arrows, the sharp light peaks that we consider could be produced by SN outbursts. The first one is that around 1970, which has been compared in Section 2.3 with an SN explosion. This event is followed by a slower decay peak (labelled A), which has been identified with the evolution of the associated cSNR. Single

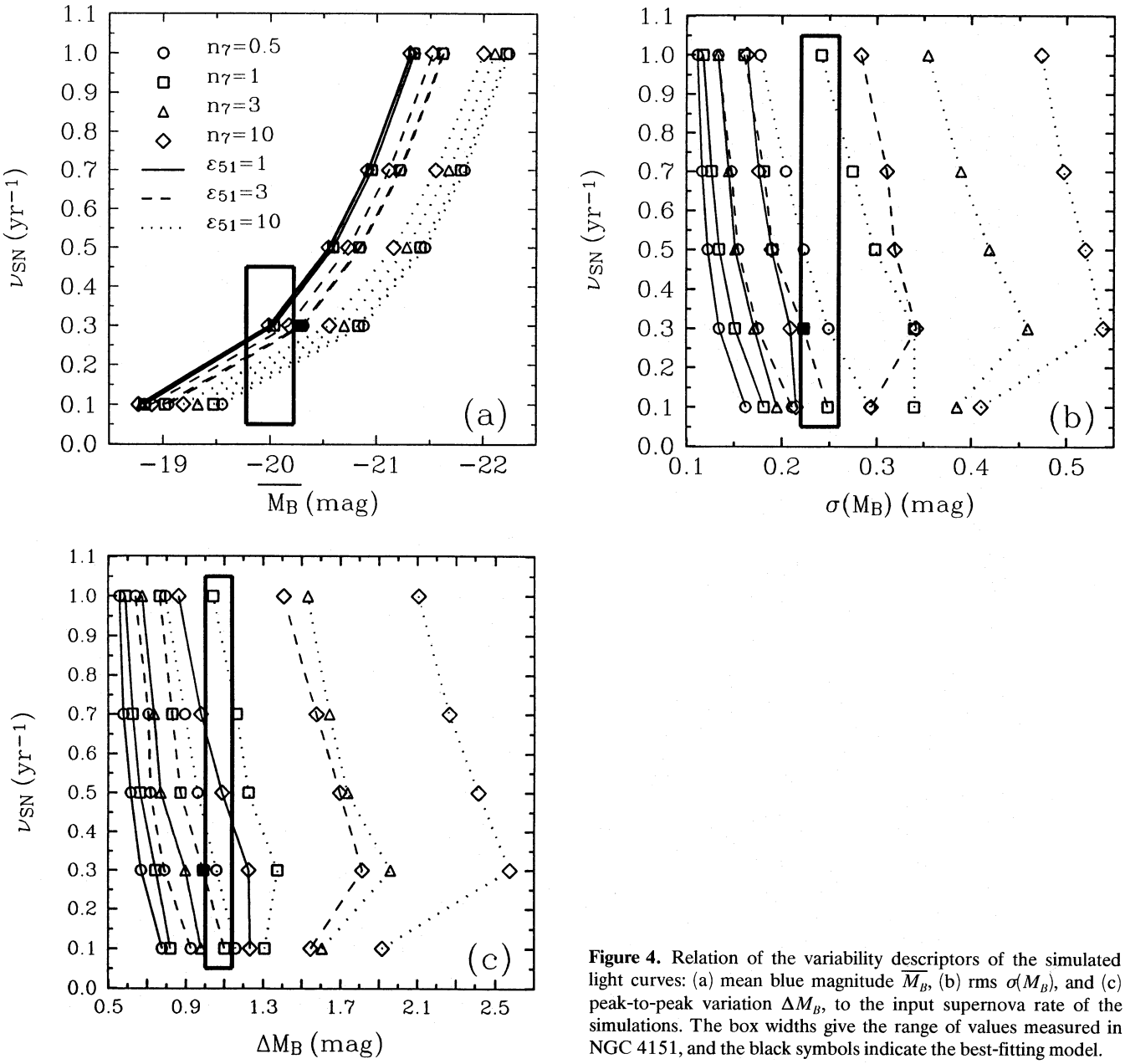

Figure 4. Relation of the variability descriptors of the simulated light curves: (a) mean blue magnitude $\overline{M_B}$, (b) rms $\sigma(M_B)$, and (c) peak-to-peak variation ΔM_B, to the input supernova rate of the simulations. The box widths give the range of values measured in NGC 4151, and the black symbols indicate the best-fitting model.

isolated events like this one are not common, although that of 1979/81 (C_2) is probably of the same type. We can observe in this variation a sharp peak followed by a slower decay decline, although the poor sampling in this region might have lost the rise to the second peak. Peaks A and C_2 are similar to peaks A^a, C^a and D^b in the simulations.

Peaks B, C and D are rounder than peaks A and C_2. It is difficult to identify which of the sharp peaks might have been the SN explosion, although the events in 1973 and 1982 seem strong candidates for the SN explosions of bumps B and D, respectively. The time interval between these sharp peaks and the peaks of the associated bumps has the same time-scale as those of A and C_2. These bumps are similar to B^a, B^b and C^b of Figs 5(a) and (b), which are superpositions of various cSNRs. From these simulated light curves (solid lines), it is obvious that identification of the sharp peaks corresponding to the SN explosions can be a hard task, without the guideline of the theoretical light curves (dotted lines), especially when the explosions occur close to one another. It would have been even more difficult if we had introduced in the simulations the secondary peaks that occur during the evolution of the remnant, which involve energies and time-scales similar to those of the SN outbursts. Although the double-peaked nature of the SN + cSNR light curve is a potential test for the model, we are not able to distinguish between secondary flares and SN explosions just by considering the light curve. In fact, peaks C_1 and E are preceded by faint bursts that could be either SN outbursts or secondary flares of the previous bumps. Nevertheless, the SN outburst of peak C_1 is probably lost, due to the poor sampling in this region, as is illustrated by peak C^a in the simulations.

At this stage, our light simulations are, nevertheless, far too simple to take account of the details in individual events. The introduction of secondary flares in the evolution of the remnants would increase the number of sharp peaks, which constitute the rapid component of variability. These secondary flares correspond to three well-identified

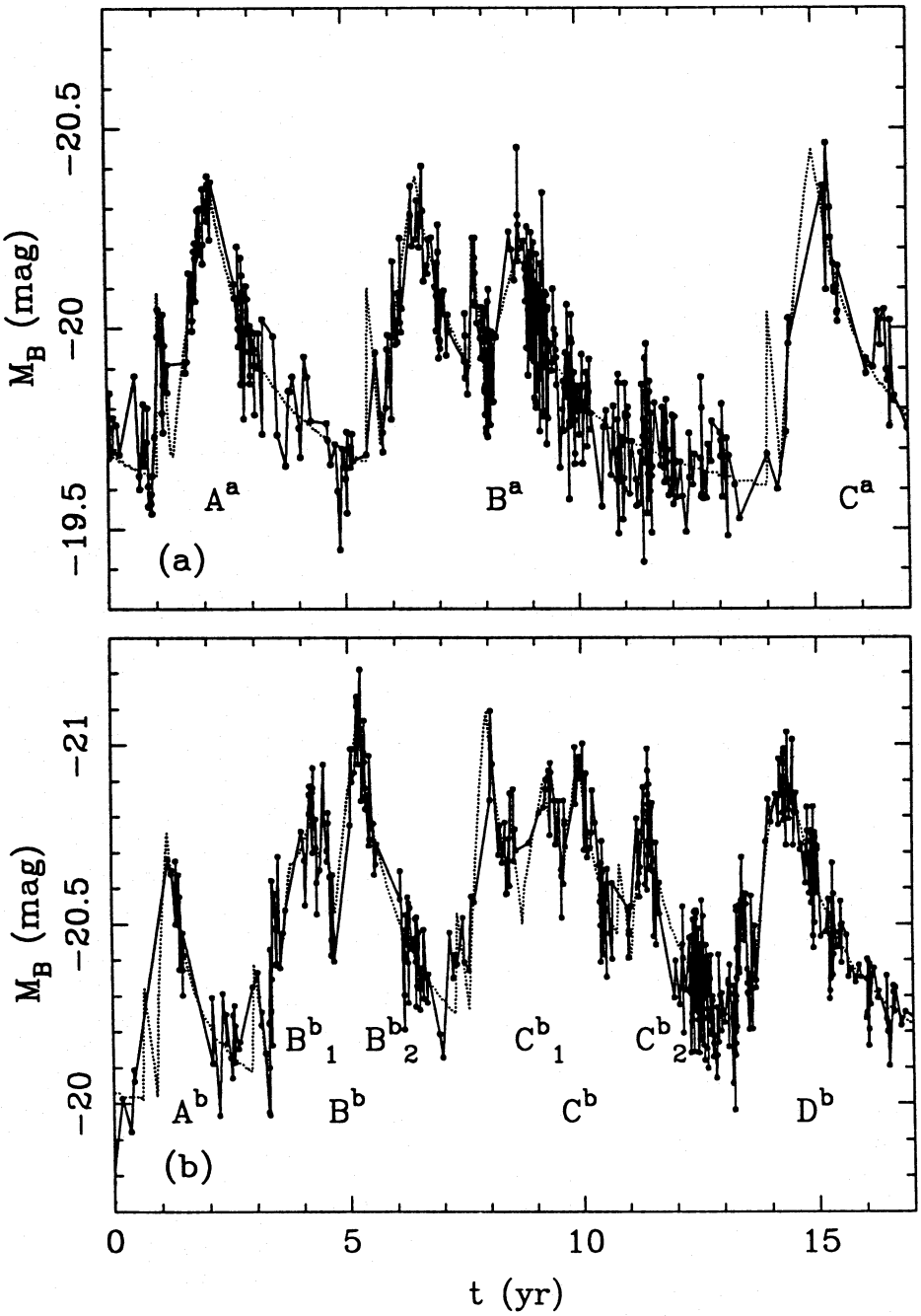

Figure 5. Simulated light curves for (a) $\nu_{SN} = 0.2\ yr^{-1}$, and random $\varepsilon_{51} = 3.0 \pm 0.9$, $n_7 = 0.5 \pm 0.1$; (b) $\nu_{SN} = 0.3\ yr^{-1}$, and random $\varepsilon_{51} = 3.1 \pm 0.9$, $n_7 = 1.0 \pm 0.3$, with a grid of points in the light curves as that of Fig. 1 and simulated observational errors of $\sigma^{obs} = 0.1$ mag. The dotted lines represent simulated light curves without errors for an ideal sample of points.

processes in the evolution of the remnant: the first is due to the outer shell formation by the leading shock, which produces a peak at maximum luminosity; the second is due to the inner shell formation by the reverse shock, and the third is due to the collision of these two shells (Tenorio-Tagle et al. 1993; Terlevich et al. 1994). On top of all this, after shell formation, there are light oscillations with time-scales of months, due to cooling instabilities (Chevalier & Imamura 1982; Bertschinger 1986). The general trend of the light evolution will continue to be $t^{-11/7}$, while the density of the circumstellar medium is roughly constant, but, as soon as the shock reaches the edge of the circumstellar medium, the luminosity will drop, following a law that depends on the density profile. The rise of the light curve of the cSNR used in this work is also a simplification of a more complicated problem. New 2D hydrodynamical models show that this increase is not linear as assumed here, but changes, for a variety of values of the density and metallicity, as $t^{0.8}$ (see also Draine & Woods 1991).

5 DISCUSSION

As we saw in the previous section, there are three input parameters in the light curve models: ν_{SN}, ε_{51} and n_7. A first

estimate of these parameters was obtained in Section 4 from the comparison of variability descriptors of the observed light curve with those of simulated ones. We will show, in this section, that the values of these parameters can also be determined from independent observations.

5.1 The supernova rate

It was shown in Section 3 that the SN rate per unit blue stellar luminosity in a young stellar cluster is almost constant for a wide range of IMFs and cluster ages. This result leads to an important prediction of the starburst model: the supernova rate and the cluster luminosity, i.e. the minimum luminosity of the light curve (when the broad lines are almost absent), are related by

$$\frac{n_{\rm SN}}{t_{\rm lc}} \sim 2\times10^{-11} L_B^{\rm min}, \tag{9}$$

where $L_B^{\rm min}$ is the B-band luminosity at minimum in solar units, $n_{\rm SN}$ is the number of SNe, and $t_{\rm lc}$ is the length of the light curve, in yr. When the AGN goes through an active phase, it shows a bright blue continuum and prominent broad lines coming from the cSNR. During minima, the variable continuum fades and the broad lines weaken, as the ejecta and the radiating shells from previous cSNR explosions cool down (Terlevich et al. 1992). Eventually, if no more SN replenishment occurs, the broad lines weaken down to the limit of disappearance, giving birth to a transient type 2 Seyfert phase, while the continuum is still blue, due to the presence of the hot stars in the underlying cluster. This could be the case of the two deep photometric minima of NGC 4151, in 1981 and 1984, in which very weak or no broad lines were detected (Antonucci & Cohen 1983; Lyutyi et al. 1984; Penston & Pérez 1984).

For high-luminosity sources, when the SN rate is higher than 1 SN yr^{-1}, the minimum of the light curve has a non-negligible contribution from the superposition of old cSNRs, and relationship (9) needs a correction. For low-luminosity systems, the determination of the SN rate is strongly affected by sampling errors, and therefore a good determination of the SN rate requires a very long observing span of time, covering many events. Assuming that the non-variable nuclear component of NGC 4151 is $M_B \approx -19.5$ mag, corresponding to the minimum in 1981 or 1984, the predicted SN rate, from Figs 3(c) and (d), is about 0.2 SN yr^{-1} for ages from 10 to 60 Myr.

On the other hand, in Section 4 we have shown that the comparison of the observed variability descriptors of NGC 4151 with the model predictions of Fig. 4 also shows the SN rate in NGC 4151 to be between 0.2 and 0.3 SN yr^{-1}, which is in agreement with the determination above. In fact, a rough estimation of the SN rate can be made directly from the observed light curve. Between 1970 and 1985, at least five, and at most six, slow-component bumps can be identified in Fig. 1. This is consistent with the expected number of peaks $n_{\rm SN} = 3 \pm 2$ at $1\,\sigma$ confidence level.

It is remarkable that these completely independent SN rate estimators, i.e. the photometric minimum light and the number of slow-component peaks of the light curve, are in such good agreement. This simple fact gives support to the model, since it fulfils the prediction that the minimum luminosity and the number of peaks of a light curve are related by (9), which has been established from the standard theory of star formation and evolution.

5.2 The energy per supernova

In the starburst model, the value of the energy per SN is an important constraint on the predicted equivalent width of recombination lines, such as Hβ. From the models of Terlevich et al. (1992), cSNRs have an average output luminosity in Hβ that accounts for about 3 per cent of the bolometric luminosity of each cSNR. The underlying continuum at λ4861 Å comes mainly from the stars of the cluster with a contribution of about $17\,\varepsilon_{51}$ per cent from the cSNRs. The time-averaged equivalent width of the broad + narrow Hβ, for AGN that show broad lines, then results:

$$\overline{W_{\rm H\beta}} \approx 40\ {\rm Å}\,\frac{\varepsilon_{51}}{1+0.17\,\varepsilon_{51}}, \tag{10}$$

independent of the SN rate and, therefore, of the total luminosity of the AGN. Furthermore, $\overline{W_{\rm H\beta}}$, like the SN rate per unit blue luminosity $\nu_{\rm SN}/L_B^*$, is almost independent of the choice of IMF; it is, nevertheless, weakly dependent on the adopted bolometric correction and on the fraction of light emitted in Hβ by a cSNR. The use of equation (10) to determine the value of ε_{51} gives a result that is independent of the adopted cosmology. We should note that, for low-luminosity variable AGN, the predicted equivalent width changes with time, being large at the maxima of the light curve and small at the minima. This effect may be the source of the type transitions observed in many AGN, in which the broad lines have temporarily disappeared, leading to quiescent Seyfert 2 stages (Aretxaga & Terlevich 1994).

The near-constancy of the time-averaged equivalent width of Hβ in AGN is a central prediction of the starburst model. Equation (10) is of fundamental importance. It indicates that the observed narrow range of values of $\overline{W_{\rm H\beta}}$ (Searle & Sargent 1968; Yee 1980; Shuder 1981; Osterbrock 1991) is due to the roughly universal value of the total energy per SN: $1 \lesssim \varepsilon_{51} \lesssim 5$ gives $40 \lesssim \overline{W_{\rm H\beta}} \lesssim 110$ Å. This is a strong prediction, almost independent of the choice of cosmology, IMF or SN bolometric correction.

In the case of NGC 4151, the time-averaged equivalent width of Hβ is about 78 ± 13 Å (Antonucci & Cohen 1983), giving an energy per SN of $\varepsilon_{51} \approx 3$, according to equation (10). This is also the value obtained from integrating the light emitted in one of the isolated slow-component peaks of the light curve. On the other hand, the energy of each cSNR, derived from the comparison of observed and simulated variability descriptors of Fig. 4, is also about 3×10^{51} erg. Energies below that value cannot explain the observed variability amplitudes, while for larger energies the variability amplitude is too large. This value of the kinetic energy per SN is similar to the best determinations for bright SNe that we have: 3×10^{51} erg for SN 1979C (Branch et al. 1981) and 1.5×10^{51} erg for SN 1987A (Woosley 1988).

5.3 The circumstellar density

From the fittings of the light curve carried out in Section 4, we determined that the circumstellar density required to reproduce the overall variability of NGC 4151 is $n_7 \approx 1$. This

is also the value that matches the second peak of Fig. 2, which we have identified with the evolution of a cSNR. Higher densities would make the evolution more peaky and lower ones would make it flatter, as derived from equation (2). The fits to the evolution of well-isolated peaks in the light curve of NGC 4151 are, therefore, in agreement with the values derived from Fig. 4. It should be noted that these circumstellar densities are similar to those determined from spectroscopic observations of cSNRs (Filippenko 1989; Stathakis & Sadler 1991).

6 SUMMARY AND FUTURE PROSPECTS

Owing to its proximity and relatively well-sampled light curve, NGC 4151 is, among galaxies with AGN, the best candidate to test the origin of the optical variability in the starburst model.

We have shown that the energies and light curves of observed supernovae and compact supernova remnants are comparable to those of the isolated peaks in the light curve of this galactic nucleus.

We have presented two important relationships of the starburst model. First, the supernova rate is related to the blue-band stellar light, independently of the initial mass function, age and/or total mass of the cluster. Secondly, the equivalent width of Hβ is related to the energy of the SN involved, independently of the initial mass function, age and/or total mass of the cluster and, furthermore, independently of the assumed cosmology. These relationships give rise to two strong predictions of the model:

(i) the number of slow-component peaks of the light curve is related to the minimum luminosity, when the broad lines are lost;

(ii) if the energy per SN has a universal value, then the equivalent width of Hβ in AGN that show broad lines should be in a narrow range of values.

To test these predictions, we did the following.

(a) We estimated the nuclear cluster luminosity in NGC 4151, assuming that, when the light reaches an absolute minimum and, simultaneously, the broad emission lines disappear from the nuclear spectrum, the observed nuclear light is dominated by the young stellar cluster. The estimated supernova rate is about 0.2–0.3 SN yr^{-1}, remarkably similar to the observed frequency of the slow-component peaks. This is a simple but robust result that gives support to the model.

(b) We computed Monte Carlo simulations of light curves, described by three input parameters: the SN rate (ν_{SN}), the energy per SN (ε_{51}) and the density of the circumstellar medium in which the explosion takes place (n_7). We showed that the global variability of the light curve of NGC 4151, measured with the mean magnitude $\overline{M_B}$, the rms $\sigma(M_B)$ and the peak-to-peak variation ΔM_B, is best fitted by simulated light curves with an SN rate $\nu_{SN} \approx 0.2$–0.3 yr^{-1}, an energy per SN of about 3×10^{51} erg, and a circumstellar density of about 10^7 cm^{-3}.

(c) We showed that the input parameters of the Monte Carlo simulations (ν_{SN}, ε_{51}, n_7) can also be determined from independent observations. The ν_{SN} is determined by the minimum of the light curve, when the broad lines are almost absent; the energy ε_{51} is determined by the equivalent width of broad recombination lines, such as Hβ, and by the total luminosity emitted in isolated peaks. The circumstellar density n_7 is determined from the rate of decay of well-sampled isolated peaks in the light curve. We have to stress the fact that these methods for determining ν_{SN} and ε_{51} are independent of those used in point (b), which considered the global variability of the light curve.

The computed light curves obtained with these parameters reproduce qualitatively, and quantitatively, the main characteristics of the observed light curve of NGC 4151, namely the mean luminosity, the number of peaks and the decay amplitudes of individual peaks, as well as the presence of slow and rapid components. We find that the long-term behaviour of the light curve of NGC 4151 is well described by the starburst model. NGC 4151 fulfils both predictions about the number of peaks and about the equivalent width of the lines.

A more extended study of the variability of AGN is clearly needed. It will be interesting to include other AGN with well-sampled light curves and a wide range of luminosities, to find out the consistency of the predictions. Other important properties of the variability, such as colour variations in the general long-term evolution and the origin of the rapid variability in UV and X-rays, are under study, and constitute the subject of separate papers.

ACKNOWLEDGMENTS

We are grateful to M. V. Penston and M. A. J. Snijders, who kindly provided us with the light curve of NGC 4151, to O. Lahav, who made available to us his code for modelling the velocity field around the Virgo cluster, and to Roberto Cid Fernandes, Marisa García-Vargas, Angeles Díaz and Elena Terlevich, for many suggestions that greatly improved this paper. IA acknowledges RGO for its hospitality, and the Basque government and the Spanish DGICYT for financial support through grant BFI88.009 and project PB900182.

REFERENCES

Allen C. W., 1973, Astrophysical Quantities. The Athlone Press, London
Alloin D., Pelat D., Phillips M. M., Fosbury R. A. E., Freeman K., 1986, ApJ, 308, 23
Antonucci R. R. J., Cohen R. D., 1983, ApJ, 271, 564
Aretxaga I., Terlevich R., 1993, Ap&SS, 205, 69
Aretxaga I., Terlevich R., 1994, in Tenorio-Tagle G., ed., Violent Star Formation: From 30 Doradus to QSO. Cambridge Univ. Press, Cambridge, in press
Barbon R., Capellaro E., Turatto M., 1989, A&AS, 81, 421
Bertschinger E., 1986, ApJ, 304, 154
Branch D., Falk S. W., McCall M. L., Rybski P., Uomoto A. K., Wills B. J., 1981, ApJ, 244, 780
Chevalier R. A., Imamura J. N., 1982, ApJ, 261, 543
Cid Fernandes R., Dottori H. A., Gruenwald R. B., Viegas S. M., 1992, MNRAS, 255, 165
Clavel J. et al., 1990, MNRAS, 246, 668
Clavel J. et al., 1991, ApJ, 366, 64
Dibaĭ É. A., Lyutyi V. M., 1984, SvA, 28, 7
Draine B. T., Woods D. T., 1991, ApJ, 383, 621
Dressler A., Lynden-Bell D., Burstein D., Davies R. L., Faber S. M., Terlevich R. J., Wegner G., 1987, ApJ, 313, 42
Filippenko A. V., 1989, AJ, 97, 726
Filippenko A. V., Terlevich R. J., 1992, ApJ, 397, L79

Franco J., Melnick J., Terlevich R., Tenorio-Tagle G., Różyczka M., 1993, in Franco J., Ferrini F., Tenorio-Tagle G., eds, Star Formation, Galaxies and the Interstellar Medium. Cambridge Univ. Press, Cambridge, p. 149
García-Vargas M. L., 1991, PhD thesis, Univ. Autónoma de Madrid
García-Vargas M. L., Díaz A. I., Terlevich E., Terlevich R., 1993, Ap&SS, 205, 77
Gill T. R., Lloyd C., Penston M. V., Snijders M. A. J., 1984, MNRAS, 211, 31
Lyutyi V. M., 1977, SvA, 21, 655
Lyutyi V. M., 1979, SvA, 23, 518
Lyutyi V. M., Oknyanskii V. L., 1987, SvA, 31, 245
Lyutyi V. M., Oknyanskii V. L., Chuvaev K. K., 1984, SvA, 10, L335
Maeder A., 1990, A&AS, 84, 139
Maeder A., Meynet G., 1988, A&AS, 76, 411
Maoz D. et al., 1991, ApJ, 367, 493
Miller G. E., Scalo J. M., 1979, ApJS, 41, 513
Niemela V. S., Ruíz M. T., Phillips M. M., 1985, ApJ, 289, 52
Osterbrock D. E., 1991, Rep. Prog. Phys., 54, 579
Penston M. V., Pérez E., 1984, MNRAS, 211, 33P
Penston M. V. et al., 1981, MNRAS, 196, 857
Peterson B. M., Ferland G. J., 1986, Nat, 342, 345
Peterson B. M. et al., 1991, ApJ, 368, 119
Phillips M. M., Hamuy M., Maza J., Ruiz M. T., Carney B. W., Graham J. A., 1990, PASP, 102, 299
Pica A. J., Smith A. G., Webb J. R., Leacock R. J., Clemens S., Gombola P. P., 1988, AJ, 96, 1215
Rieke G. H., Lebofsky M. J., 1981, ApJ, 250, 87
Sandage A., Tammann G. A., 1981, A Revised Shapley–Ames Catalog of Bright Galaxies. Carnegie Institution of Washington, Publ. 635
Schlegel E. M., 1990, MNRAS, 244, 269
Searle L., Sargent W. L., 1968, ApJ, 153, 1003
Shields J., 1992, ApJ, 399, L27
Shuder J. M., 1981, ApJ, 244, 12
Shull J. M., 1980, ApJ, 237, 769
Smith A. G., Nair A. D., Clemens S. D., 1991, in Miller H. R., Wiita P. J., eds, Variability of Active Galactic Nuclei. Cambridge Univ. Press, Cambridge
Smith A. G., Nair A. D., Leacock R. J., Clemens S. D., 1993, AJ, 105, 437
Snijders M. A. J., 1991, in Duschl W. J., Wagner S. J., Camenzind I., eds, Variability in Active Galaxies. Springer-Verlag, Berlin, p. 9
Stathakis R. A., Sadler E. M., 1991, MNRAS, 250, 786
Tenorio-Tagle G., Terlevich R., Różyczka M., Franco J., Melnick J., 1993, in Franco J., Ferrini F., Tenorio-Tagle G., eds, Star Formation, Galaxies and the Interstellar Medium. Cambridge Univ. Press, Cambridge, p. 153
Terlevich R., 1990, in Fabbiano G., Gallagher J. S., Renzini A., eds, Windows on Galaxies. Kluwer, Dordrecht, p. 87
Terlevich R., Melnick J., 1985, MNRAS, 213, 841
Terlevich R., Melnick J., 1988, Nat, 333, 239
Terlevich R., Melnick J., Moles M., 1987, in Khachikian E. Ye., Fricke K. J., Melnick J., eds, Proc. IAU Symp. 121, Observational Evidence of Activity in Galaxies. Reidel, Dordrecht
Terlevich R., Tenorio-Tagle G., Franco J., Melnick J., 1992, MNRAS, 255, 713
Terlevich T., Tenorio-Tagle G., Franco J., Różyczka M., Melnick J., 1994, MNRAS, submitted
Turatto M., Cappellaro E., Danziger I. J., Benetti S., Gouiffes C., Della Valle M., 1993, MNRAS, 262, 128
Ulrich M.-H., Boksenberg A., Bromage G. E., Clavel J., Elvius A., Penston M. V., Perola G. C., Snijders M. A. J., 1991, ApJ, 382, 483
van den Bergh S., 1988, AJ, 96, 701
Wheeler J. C., Mazurek T. J., Sivaramakrishnan A., 1980, ApJ, 237, 781
Woosley S. E., 1988, in Kafatos N. M., Michalitsianos A., eds, Supernova 1987A in the Large Magellanic Cloud. Cambridge Univ. Press, Cambridge, p. 289
Yee H. K. C., 1980, ApJ, 241, 894